Elektrotech. Inftech. (2022) 139:139–148
https://doi.org/10.1007/s00502-022-01006-3

e+i elektrotechnik und informationstechnik

PCB motors for sub-fractional HP auxiliary fan drives: a feasibility study

David Auer · Stefan Leitner · Annette Muetze

Received: 22 December 2021 / Accepted: 31 January 2022 / Published online: 23 March 2022

Abstract This paper investigates the use of PCB motors for sub-fractional HP auxiliary fan drives. First, the basic idea of PCB motors as well as the main advantages and disadvantages are discussed, followed by the description of the design process for a PCB motor for a small automotive fan application. Three different stator designs have been implemented, each on a 4-layer PCB. Finally, the paper gives an overview of the measurements performed and the results obtained for the prototypes of the manufactured PCB motors and suggests design improvements.

Keywords Automotive applications · Auxiliary drives · Axial flux motor · Printed circuit board · Sub-fractional horsepower drives · Three-phase BLDC motor

PCB-Motoren für Kleinstantriebe in kleinen Lüfteranwendungen: eine Machbarkeitsstudie

Zusammenfassung Dieser Beitrag untersucht die Verwendbarkeit von PCB-Motoren für Kleinstantriebe, im Besonderen für kleine Lüfteranwendungen. Zu Beginn wird auf den grundsätzlichen Aufbau von PCB-Motoren sowie deren primäre Vor- und Nachteile eingegangen. Danach wird der Designprozess für einen PCB-Motor, der als Antrieb für einen kleinen automobilen Lüfter eingesetzt werden soll, beschrieben. Es wurden drei verschiedene Ständerdesigns umgesetzt, je auf einer 4-Layer-Leiterplatte. Abschließend werden die an den Prototypen der Motoren durchgeführten Messungen sowie Messergebnisse, diskutiert und Verbesserungsmöglichkeiten aufgezeigt.

D. Auer (✉) · S. Leitner · A. Muetze, OVE
Electric Drives and Machines Institute, Graz University of Technology, Inffeldgasse 18/1, 8010 Graz, Austria
d.auer@student.tugraz.at

Schlüsselwörter Automobile Anwendungen · Hilfsantriebe · Axialflussmotor · Leiterplatte · Kleinstantriebe · Dreiphasiger BLDC-Motor

1 Introduction

For many applications, such as small mass-produced cooling devices, sub-fractional horsepower drives (up to 10 W) are used. The main advantages of these drives are simple and cheap manufacturing. As these drives are used in automotive applications, they should have low wear and tear, thus be maintenance-free. This can be achieved with brush-less permanent magnet motors. With the goal of a simple assembly of the motor, axial-flux printed circuit board (PCB) motors are studied for such cooling fan applications, consisting of a PCB stator and a permanent magnet rotor. This paper investigates the feasibility of a PCB motor for an automotive radial fan application. The motor is designed, and the feasibility is verified by experimental methods.

2 Principle Idea of PCB Motors

The main idea of PCB motors is to replace conventional copper wire windings of standard electric motors with printed circuit boards. Increased flexibility in winding design, while at the same time decreased manufacturing costs are one of the main goals. Most of the commonly used electric motors are of radial-flux type, this means that the main magnetic flux in the air-gap is aligned in radial direction. The manufacturing processes for these motor designs are well known and have been established in industrial manufacturing for a long time [1]. For these machines, the windings form a three dimensional shape in the stator. Such windings could hardly be achieved by standard PCBs. Some research on the use of flexible PCBs for

radial-flux machines is presented in [2] and [3]. Axial-flux machines, in contrast, have a winding design suitable for PCB printing. For this type of electric motor, the main magnetic flux in the air-gap is arranged in axial direction, so, parallel to the rotational axis. The main functional principle is the same as for radial-flux machines.

The maximum torque generated by a radial-flux machine is proportional to its volume, i.e., to the square of its rotor radius times its length. For axial configurations, in contrast, the torque increases proportional to the cube of its outer radius [1].

In terms of PCB motors, this arrangement means a printed circuit board as stator, containing all windings, and a permanent magnet rotor stacked on top of each other. The stator does not contain an iron core. Many different configurations of axial-flux machines have been proposed, with multiple stators, as well as multiple rotors. The simplest one consists of one stator with a single rotor and is used in this study.

2.1 Advantages of PCB Motors

High flexibility in stator design: Since the stator of a PCB motor consists of a printed circuit board, a new coil configuration can easily be designed and manufactured. The PCBs for stator coils can be designed in every standard PCB design software, and therefore, a new design variant can be drawn easily. Prototype manufacturing for PCBs typically only takes a few days, and so, within a short time a new prototype can be made available. Also, multiple stator designs can be ordered at once and exchanged to provide different testing setups and identify the configuration which suits the application best. This is much simpler than the process for standard motors with copper wire windings and a laminated iron core, where time and cost intensive prototyping would be necessary [4].

Highly scalable and fast manufacturing process: As PCB manufacturing is a standard and high-volume industrial process, large batches of PCB stators can be produced within a short time. Another advantage of similar character is the assembly process. No specially designed production lines for wire winding are necessary, the PCBs can be manufactured at every standard PCB manufacturer. Also, an assembly line for PCB motors would be more flexible than for standard motors. For example, if the application needs a different power output and therefore stator configurations, simply different PCBs could be fed into the assembly line and mounted, just as the type before since the physical dimensions of the PCBs may possibly stay the same [4].

No iron losses in the stator: The PCB is made of FR4 (flame retardant glass reinforced epoxy) material, which has a relative permeability μ_r of nearly 1 and no hysteresis curve [5]. Since the PCB stator has no iron core (and if there is no back iron mounted beneath the stator), generally no iron losses, i.e., hysteresis and eddy current losses, occur. Yet, eddy current losses can still occur in the printed copper winding as a result of the changing magnetic field when the rotor is spinning [5].

No cogging torque: The stator of the PCB motor has no slotted iron core. Hence, the cogging torque (which is defined as the interaction of the permanent magnets on the rotor with a slotted iron stator structure in the no-load condition) is zero. Cogging torque can lead to torque ripple as well as speed ripple [4].

Integration of control circuit: The necessary control and supply circuits to operate the motor can be integrated onto the same PCB as the stator is made of. This saves space and makes the motor overall smaller.

Lower space requirement in axial direction: Due to the design as an axial-flux machine, these motors can be built using less space in axial direction compared to radial flux machines. It makes them suitable for low profile applications [6].

2.2 Disadvantages of PCB Motors

Lower torque density: Compared to standard motors with copper wire windings and an iron core, the magnetic field is much lower due to the large effective air-gap. Lower magnetic field-strength means also a lower force on the rotor and therefore a lower torque for a fixed volume, i.e., a lower torque density [5].

Lower winding density: Depending on the number of layers chosen for PCB manufacturing, only a limited number of turns can be placed. The more layers the PCB contains, the more turns can be fit within each coil. As every conducting layer has to be separated by an insulation layer, which has a defined thickness, the different layers are exactly in this distance and therefore far apart from each other. In contrast, for copper wire windings, the wires often lie directly next to each other with a minimum insulating coating in between [5].

Higher ohmic resistance in stator: Only certain values are available for copper thickness on PCBs in standard manufacturing processes. Typically, these are between 15 μm and 200 μm. Therefore, the traces have quite a low cross section and thus high ohmic resistance per unit length. This issue can be addressed by different connection methods of the different layers. For example, if the coils on each layer are connected in series, the ohmic resistance of each individual layer adds up while if in parallel connection the overall ohmic resistance can be kept low [5].

Strong permanent magnets needed: Due to the absence of an iron core and thus a rather large magnetic resistance in the flux path, strong permanent magnets are needed on the rotor to generate the needed torque. These magnets are quite expensive and therefore add additional costs [7].

3 Design of a PCB Motor for an Automotive Radial Fan Application

The PCB motor type investigated for this paper is required to be cheap to manufacture and thus requires very few assembly steps. As a consequence, a single-rotor, single-stator design is used. The dimensions for the stator are on one hand determined by an existing housing within which the stator should fit and on the other hand by the positions of the magnets on the rotor. The useful area for winding placement is given by the active magnetic area of the magnets mounted to the rotor. With the inner and outer diameter given, a shape for the coils had to be chosen. For this prototype it was decided to fit as many turns within this available area as possible. The area of the stator is separated into circle segments of same angle. The three different designs have 6/9/12 coils, resulting in circle segments of 60/40/30 (mechanical) degrees with each segment containing one coil. The coils are connected in a three-phase star connection arrangement. Three different rotor designs have been designed.

3.1 Stator (PCB) Design

The coil's shape (see, e.g., Fig. 1) had been designed in a CAD tool and imported into the PCB design software. In coil design, on the one hand the number of turns should be as large as possible, while on the other hand a large number of turns means a higher

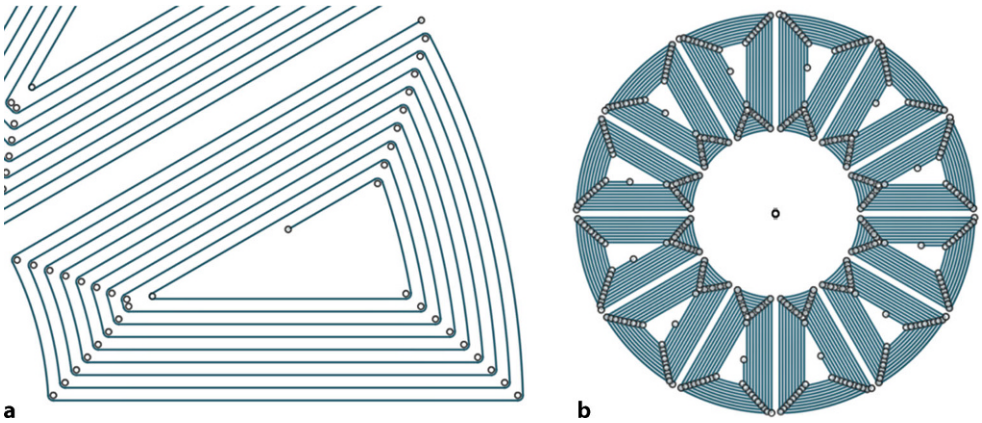

Fig. 1 12 coil PCB: coil geometry of the upper layer **(a)** and view of all coils of the upper layer **(b)**

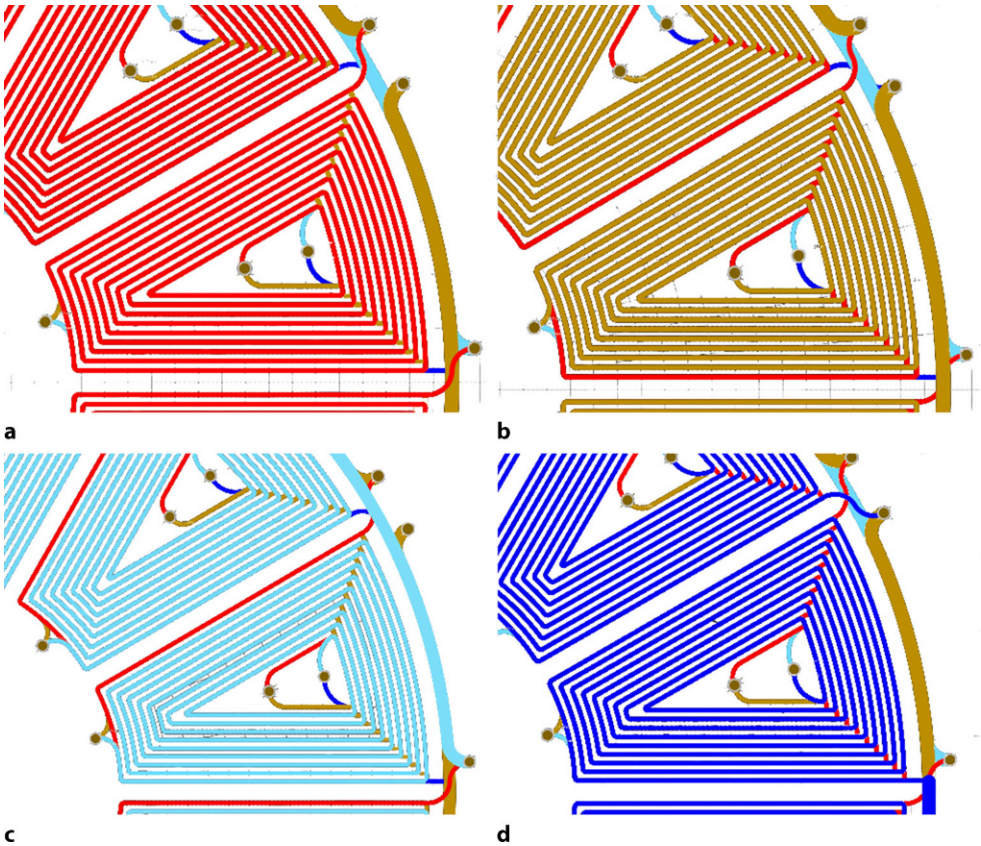

Fig. 2 Different coil layers of the 12 coil PCB: top layer **(a)**, inner layer 1 **(b)**, inner layer 2 **(c)** and bottom layer **(d)**

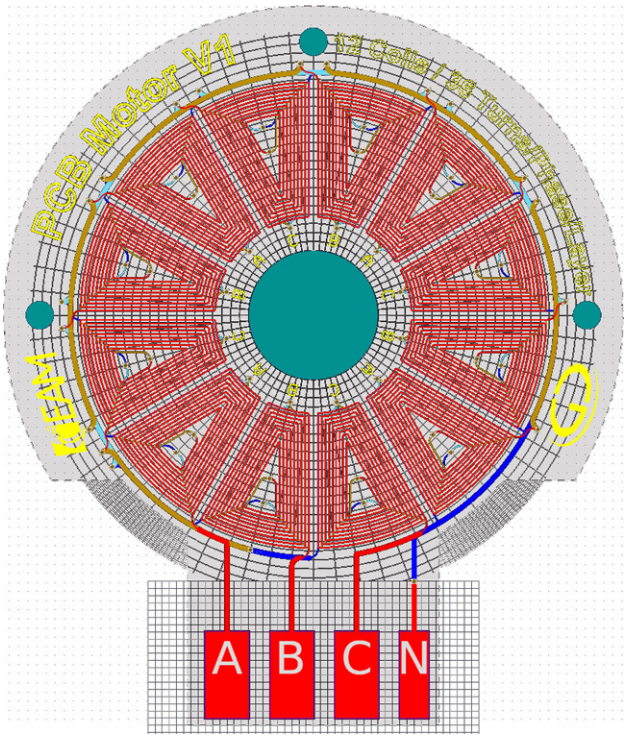

Fig. 3 Finished PCB design for the 12 coil PCB motor

ohmic resistance. To lower the resistance wider tracks on the PCB would be necessary, since the ohmic resistance of a track is given by $R = \frac{l \cdot \rho}{A}$ [8], with the length l, the cross-section A, and the specific copper resistance ρ. Wider tracks on the other hand would mean that every turn of the coil would require more space and therefore, fewer turns would be possible. Therefore, a compromise had to be found. The best effect coils would have is if the neighbour turns would be directly next to each other, but since there needs to be some space for isolation between them this space is limited. As the first design should have low production costs some limitations imposed by the manufacturer's capabilities had to be looked after. The most important ones were:

- minimal trace distance: 0.1 mm
- minimal via dimension: 0.3 mm
- minimal trace width: 0.1 mm

Therefore, the distance between the traces of the turns within the coils is exactly 0.1 mm. Since the voltage differences between each turn would be very low, no isolation problem should occur. The outer most turn of each coil is determined by the coil's outline, while the number of turns had been determined by the targeted resistances, but since the number of turns per coils should be equal for each design, this was the main criteria to decide the number of turns per coil.

In order to increase the magnetic field strength of every single coil, a 4-layer PCB was used. Each layer contains a similar coil arrangement, as shown in Fig. 1. Fig. 2 shows the different layers of one single coil. For the inner layer 1 and the bottom layer, the coils are mirrored to ensure the current is flowing in the same direction and thus enhance the magnetic field. The different layers are connected by vias. For this design concentrated windings were used, another option would be to shift different phases to different layers and realize distributed windings.

The coils are connected as a three-phase system in star configuration. To enable additional measurement possibilities, the star point has also been made accessible as a connector.

An overview of the whole PCB for the 12 coil PCB motor is shown in Fig. 3.

3.2 Rotor Design

Three different rotors (i.e., Rotors 1–3) have been manufactured and tested, see Figs. 4 and 5: Rotor 1 consists of 8 disc-shaped permanent magnets (magnetized in the axial direction) arranged on an iron washer which acts as a back iron for the magnetic flux. Each magnet has a diameter of 9 mm and an axial thickness of 3 mm. The flux density on the surface of the magnets measured by a Hall sensor amounts to about 280 mT, which decreases to 200 mT at a distance of 1 mm from the surface. The frame is mounted to a shaft which fits into a bearing mounted on the stator. Fig. 4 shows an illustration of Rotor 1 with the 8 magnets mounted.

Rotor 1 was used for a verification of the working principle with all three PCB designs. To prove the functionality under application similar conditions,

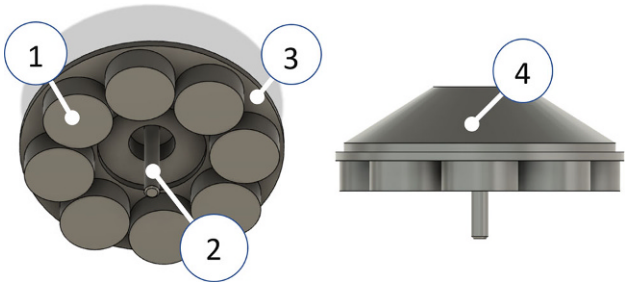

Fig. 4 Illustration of Rotor 1, which has no fan blades, consisting of permanent magnets (*1*), a shaft (*2*), a back iron washer (*3*), and a frame (*4*)

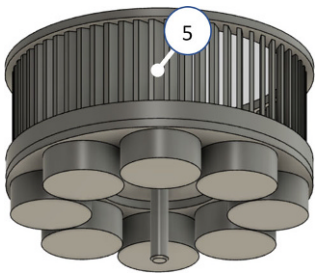

Fig. 5 Illustration of Rotor 2 with fan blades (*5*)

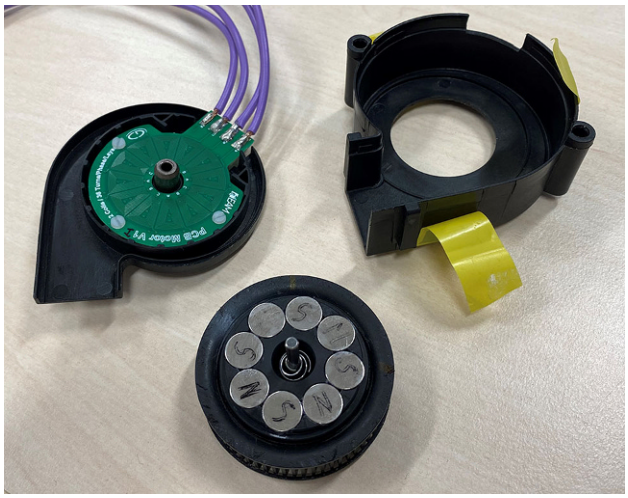

Fig. 6 Base plate with PCB, Rotor 2 and fan housing (configuration 4)

Rotor 2 and Rotor 3 have been implemented with fan blades.

For Rotor 2, the same magnets as for Rotor 1 were used, but in contrast to Rotor 1, Rotor 2 has no back iron mounted (the same holds true for Rotor 3). The measured flux density for Rotor 2 is 224 mT on the magnet's surface, which decreases to 147 mT at a distance of 1 mm from the surface.

Rotor 3 is basically the same as Rotor 2, with the only difference that the permanent magnets have a reduced thickness, i.e., 1 mm instead of 3 mm. The flux density on their surface was measured as 94 mT and decreased to a value of 64 mT at a distance of 1 mm.

3.3 Assembly

In total, 5 different motor configurations were realized, see Table 1. The PCB stator is mounted to the base plate of the housing by the use of Teflon screws. This base plate contains the slide bearing, which supports the rotor. On top, the cover of the housing completes the assembly. The components for the fan drive are presented in Fig. 6.

For all configurations the air-gap between the magnet's surface and the PCB stator was set to 1 mm.

3.4 Motor Design Parameters

During the design procedure, the following parameters for the three stator designs have been calculated.

Table 1 Realized Motor Configurations

Configuration No.	PCB	Rotor
1	6 Coils	Rotor 1
2	9 Coils	Rotor 1
3	12 Coils	Rotor 1
4	12 Coils	Rotor 2
5	12 Coils	Rotor 3

As mentioned before, the number of turns, as well as the phase resistance of the different stator designs was kept within the same range to be able to compare the motors.

Number of turns per phase: The number of turns per phase is equal for all three stator designs.

Average coil area: The sum of all areas enclosed by each turn of the PCB coils, divided by the number of turns.

The average coil area is relevant, as it correlates with the back-EMF (BEMF), i.e., induced voltage. The induced voltage in a single turn is given by [8]:

$$u_{\mathrm{ind,turn}} = -\frac{d\Phi}{dt} \tag{1}$$

with the change of the magnetic flux through that turn in respect to time. The total induced voltage depends on multiple aspects: the exact distribution of the magnetic field within every single turn of each coil, the speed of the rotation, the connection of the single coils as one phase, the magnetic field-strength and distribution of the used magnets, and the shape of the magnets as well as the coils.

Estimation of BEMF voltage: An attempt was made to analytically estimate the peak BEMF voltage. For this task some assumptions were made and hence the calculated value gives only a raw estimation of BEMF voltage to be expected during testing. For the BEMF voltage the change of the magnetic flux within the coil cross sections has to be calculated. The permanent magnets were modelled with a constant field strength. To further simplify the calculations, the round arrangement of the stator coils was split up to a linear configuration. For example, for the design with 12 coils and a rotational speed of 4700 rpm a peak phase-to-neutral voltage of 2.7 V was calculated, which would result in a BEMF constant of 5.48 $\frac{\mathrm{mVs}}{\mathrm{rad}}$.

Winding factors: Due to the varying spacial distributions of the coils in the studied designs, their winding factors differ. While the voltages induced in the

Table 2 Number of Turns

PCB	Turns per layer per coil	Turns per coil	Turns per phase
6 Coils	18	72	144
9 Coils	12	48	144
12 Coils	9	36	144

Table 3 Average Coil Area per Phase

PCB	Average coil area per layer per coil	Average coil area per layer
	mm^2	mm^2
6 Coils	43.86	87.72
9 Coils	33.41	100.22
12 Coils	26.37	105.49

Table 4 Calculated Winding Factors

PCB	Winding Factor
6 Coils	1
9 Coils	0.96
12 Coils	1

Table 5 Calculated Phase Resistances

PCB	Phase resistance
	Ω
6 Coils	22.7
9 Coils	21.1
12 Coils	20.2

coils of a phase are in phase for the 6 and 12 coil motors, there is a phase shift for the 9 coil motor. Table 4 presents the calculated winding factors.

Phase resistance: The phase resistance was calculated by the length of the track multiplied by the specific resistance of copper divided by the track's cross section,

$$R_{\mathrm{ph}} = \frac{l \cdot \rho_{\mathrm{cu}}}{A} \tag{2}$$

with the phase resistance R_{ph}, the length of the track of one phase l, the specific resistance of copper ρ_{cu} and the cross section of the track $A = w \cdot h$ (width of the track w and height of the track h). The PCBs are manufactured with a copper thickness of 1 oz which equals 35 μm. The width of all tracks of the coils is 0.15 mm. For these calculations, an ambient temperature of 20 °C was assumed, consequently, the computed specific resistance used for these calculations is $\rho_{\mathrm{cu}} = 1.786 \cdot 10^{-2} \frac{\Omega\,\mathrm{mm}^2}{\mathrm{m}}$.[8]

Table 5 presents the calculated values for the phase resistances.

As can be seen from Tables 2, 3, and 5, the three different stator designs have an equal number of turns per phase, quite similar calculated phase resistances and also the middle coil areas are within a similar range.

Realized PCBs: Fig. 7 shows the realized PCBs, as they arrived from the manufacturer.

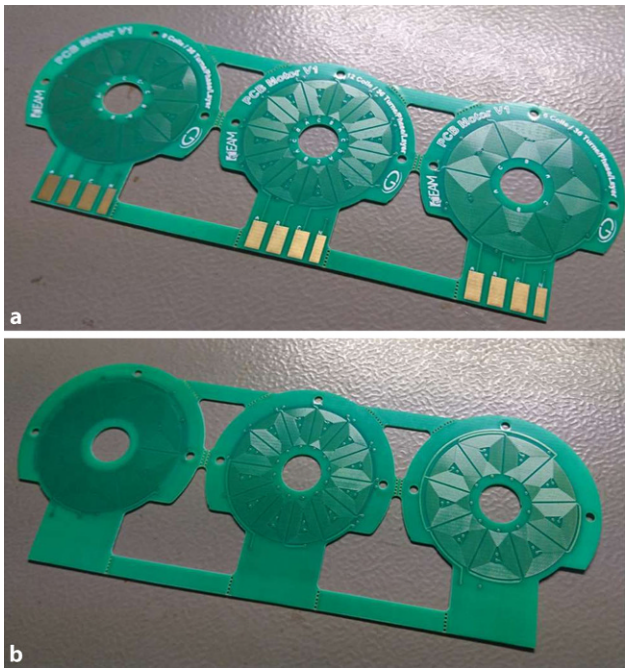

Fig. 7 PCBs on panel top view (**a**), bottom view **(b)**

4 Concept Validation

To prove the feasibility of the concept, selected measurements have been performed. The BEMF constant, phase inductance and phase resistance, which are important parameters to describe a permanent magnet motor have been evaluated. To spin the motor, it was connected to a sensor-less brush-less DC motor controller. The controller uses the measured BEMF voltage to determine the position of the rotor in relation to the stator and thus is able to control the motor. The target rotational speed was set via a potentiometer, connected to the control circuit. As the target application uses a supply voltage of 13.5 V, all further test were conducted with a DC supply voltage of 13.5 V. An overview of the measurement setup is illustrated in Fig. 8.

4.1 Measurement Results

Phase resistance: The phase resistances have been determined by means of current and voltage measurements when supplied from a DC source. (The results have been verified by a multimeter set to resistance mode.) The measured values for the phase resistances are presented in Table 6.

Compared to the values calculated during the design process (see Table 5) these values are up to 4 Ω lower which can be explained by the PCB manufac-

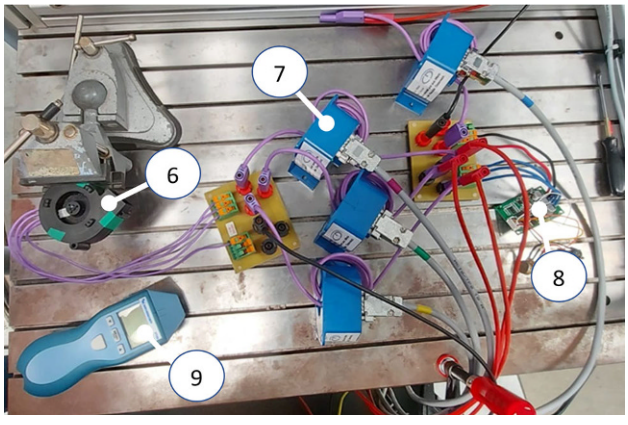

Fig. 8 Measurement setup: PCB motor (*6*), current sensor (*7*), motor controller (*8*) and optical speed meter (*9*)

Table 6 Measured Phase Resistance

PCB	R_{AB}	R_{BC}	R_{CA}
	Ω	Ω	Ω
6 Coils	36.1	36.2	36.2
9 Coils	34.1	33.9	33.9
12 Coils	32.1	31.9	31.8
PCB	R_{AN}	R_{BN}	R_{CN}
	Ω	Ω	Ω
6 Coils	18.1	18.1	18.3
9 Coils	16.9	17.2	17.2
12 Coils	16.1	16.1	15.9

Table 7 Measured Phase Inductance

PCB	L_A	L_B	L_C
	μH	μH	μH
6 Coils	87.69	87.58	86.67
9 Coils	61.78	61.75	61.61
12 Coils	43.95	44.06	43.58

turer's production tolerances which only specify minimum copper thickness.

Phase inductance: Another important parameter for a brush-less DC motor is the phase inductance. An RLC meter was used to determine the values. The RLC measurement identified the following values: The results have been verified with AC as well as voltage step measurements.

As the results in Tables 6 and 7 show, the phase inductance is relatively low in comparison to the phase resistance (in the operating range of interest). With the frequencies this motor is operated on, this means a $\cos(\varphi)$ close to 1.

BEMF constant: To determine the BEMF constant, the motor was operated at a certain speed and then switched off, measuring the phase-to-phase voltages and phase-to-neutral voltages by a data recorder during the coast down.

The calculation of the phase-to-neutral BEMF constant is based on the following equations [9]:

$$k_{\mathrm{EMF,mech}} = \frac{u_{\mathrm{pk,ph\text{-}neutral}}}{\omega_{\mathrm{mech}}} \tag{3}$$

$$\omega_{\mathrm{mech}} = f_{\mathrm{mech}} \cdot 2 \cdot \pi = \frac{n}{60} \cdot 2 \cdot \pi \tag{4}$$

with the BEMF constant $k_{\mathrm{EMF,mech}}$, peak value of the phase-to-neutral voltage $u_{\mathrm{pk,ph\text{-}neutral}}$ and angular rotational speed in mechanical degrees ω_{mech}. The same calculations were performed with the phase-to-phase voltages.

The measured BEMF phase-to-neutral voltages at 4774 rpm for the motor with 12 coils are shown in Fig. 9.

The BEMF voltage was measured for five different rotational speeds for every PCB stator with Rotor 1, showing the expected linear increase with increasing speed, see Fig. 10. The rotational speed was on one hand calculated from the waveforms of the measured

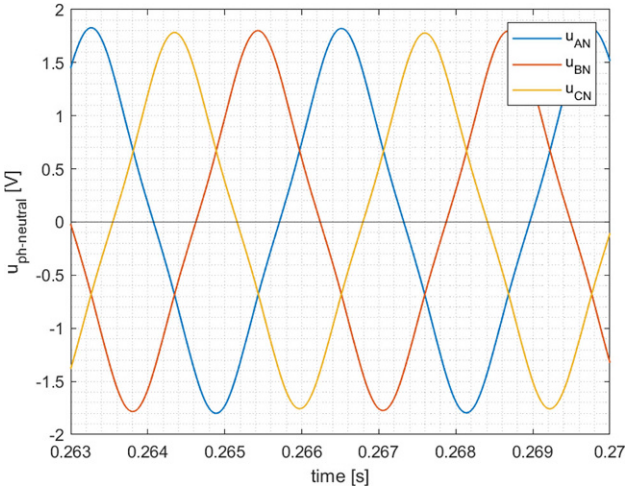

Fig. 9 Measured BEMF phase-to-neutral voltages at n = 4774 rpm for the motor with 12 coils and Rotor 1

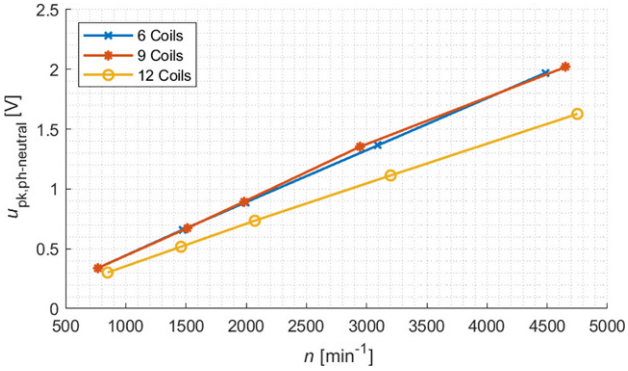

Fig. 10 BEMF voltage over speed n with Rotor 1

voltages and on the other hand verified by an optical speed meter used during the measurements.

With the peak voltages and mechanical circular speeds measured, the BEMF constant could be calculated. Since the calculations had been done at different speeds (five points for each motor) the slope of these curves gives the BEMF constant.

Table 8 shows all results of BEMF calculation for all tested motor configurations.

An analysis of the harmonic frequencies occurring in the BEMF phase-to-neutral voltages is shown in Fig. 11. The values were measured at slightly different speeds and afterwards scaled linearly to 5000 rpm to be able to compare them. The left plot shows the

Table 8 Experimentally Determined BEMF Constants

Configuration No.	BEMF constant phase-to-neutral	BEMF constant phase-to-phase
	$\frac{\mathrm{mVs}}{\mathrm{rad}}$	$\frac{\mathrm{mVs}}{\mathrm{rad}}$
1	4.41	7.3
2	4.25	7.36
3	3.22	5.85
4	3.79	6.57
5	1.48	2.57

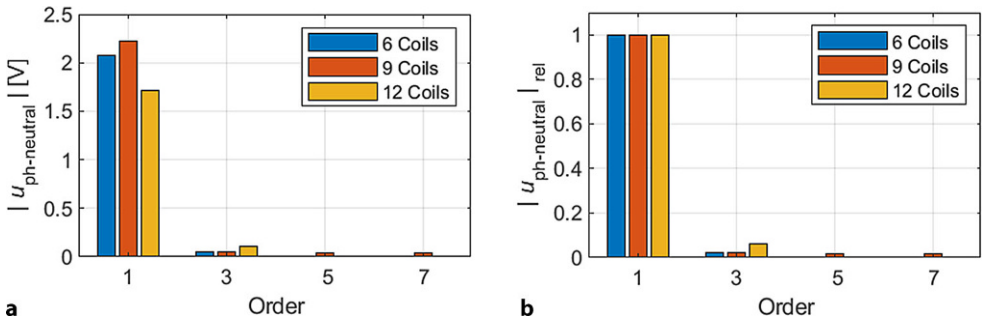

Fig. 11 Analysis of harmonics in BEMF voltages for all PCB designs with Rotor 1, scaled to 5000 rpm. Absolute values **(a)** and relative values **(b)**

Table 9 Estimated Motor Torque and Efficiency of the Studied Motor Configurations

Configuration No.	n	$I_{\mathrm{ph,RMS}}$	$P_{\mathrm{in,el}}$	M_{mot}	η
	rpm	mA	W	mNm	%
1	4484	130	1.42	1.02	33.7
2	4654	137	1.43	0.93	31.6
3	4774	158	1.66	0.96	28.9
4	4712	275	4.55	1.79	19.4
5	3282	313	5.39	1.32	8.4

absolute values. Compared to the design with 6 coils, the BEMF fundamental component is 7.2% higher for the design with 9 coils and 17.2% lower for the design with 12 coils. On the right plot the values are normalized to the amplitude of the base frequency. For example, the amplitude occurring at three times the base frequency is for the motor with 6 Coils: 2.3% / 9 Coils: 2.4% / 12 Coils: 6.1% of the amplitude at the base frequency.

Motor torque: The torque produced by the PCB motor can be estimated by $M_{\mathrm{mot}} = \frac{P_{\mathrm{in,el}} - P_{\mathrm{cu}}}{2 \cdot \pi \frac{n}{60}}$, with the rotational speed n in rpm. For these calculations only the copper losses have been considered since they dominate. All further losses, such as iron losses, and losses due to air friction and bearing friction have been neglected. The estimated values for the motor torque M_{mot} and efficiency η for the different motor configurations are presented in Table 9.

As per Table 9, for configurations 4 and 5, higher currents are needed to reach the desired speed. This can be explained on the one hand, by the absence of the back iron for the used rotors Rotor 2 and Rotor 3, as well as the fact that these rotors contain the fan

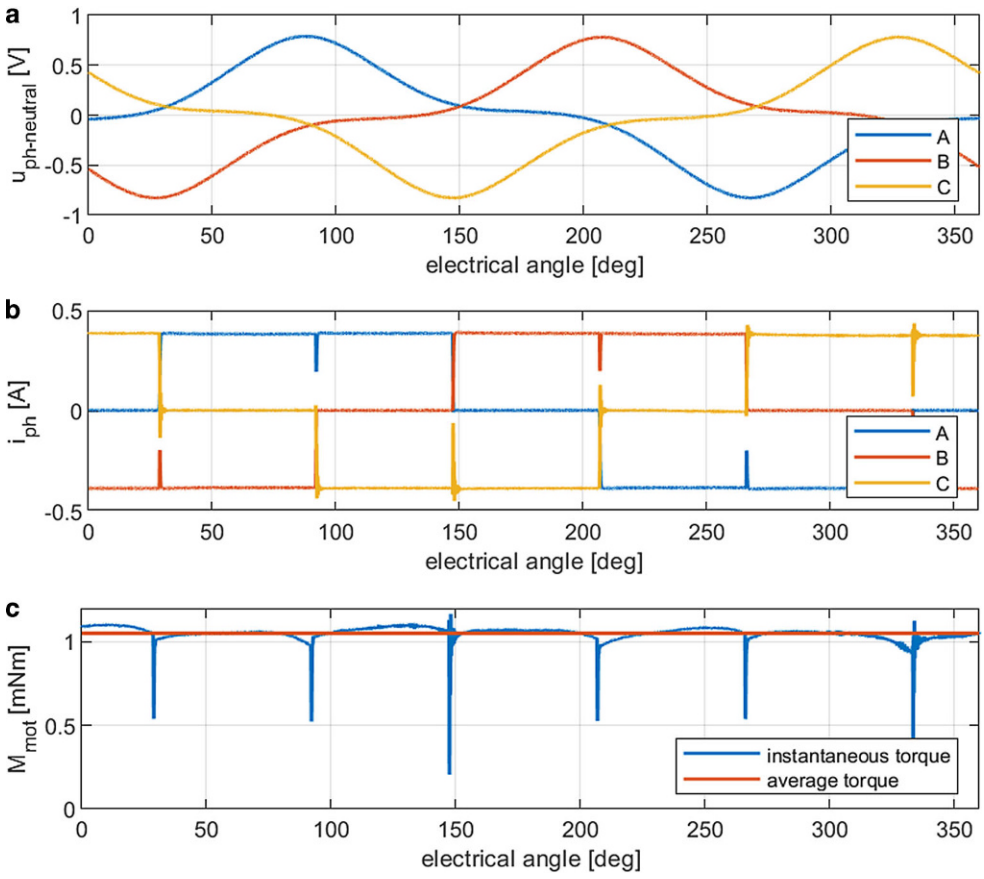

Fig. 12 Analysis of instantaneous torque for configuration 5, **a** measured BEMF phase voltage, **b** measured phase currents, **c** computed torque waveform

blades, which add additional drag to the rotor. These higher currents result in a lower efficiency, due to the high ohmic resistance of the stator coils.

Exemplarily, the determination of the torque waveform of Rotor 3 on the PCB with 12 coils (configuration 5) based on the measured current and BEMF voltage waveforms for a speed of $n = 3261$ rpm is shown. The results are presented in Fig. 12, illustrating the measured phase-to-neutral BEMF voltages (Fig. 12a), measured phase currents (Fig. 12b), and the instantaneous torque (Fig. 12c) calculated according to $M_{\mathrm{mot,inst}} = \frac{(u_{\mathrm{BEMF,ph,A}} \cdot i_{\mathrm{ph,A}}) + (u_{\mathrm{BEMF,ph,B}} \cdot i_{\mathrm{ph,B}}) + (u_{\mathrm{BEMF,ph,C}} \cdot i_{\mathrm{ph,C}})}{\omega}$. The phase current waveforms are of square shape as expected, showing dips every 60° electrical, which result from the commutation. The same dips are also visible in the instantaneous torque, see Fig. 12c. In addition, the average output torque is indicated, amounting to about 1.1 mNm for the studied operating point of the fan drive.

5 Conclusion

This paper studied the use of PCB motors for sub-fractional auxiliary fan drives. The measurements proved the basic working principle of this very simple PCB motor. The motor already reached operating points which are feasible for the target application. In order to use it in a large scale application several improvements are necessary. To increase the produced torque and at the same time reduce the ohmic losses in the stator a different connection for the single coils would be necessary, for the studied design the coils are all connected in series connection. Another option would be to use thicker copper inlays in the PCB, which would add additional costs. The rotor design can also be improved, e.g., when the single magnets are replaced by a magnetized annulus where the magnetized areas have the same shape as the coils for example. With an improved design and thus higher efficiency, such a motor type might be suitable for some sub-fractional horsepower automotive fan applications.

Funding Open access funding provided by Graz University of Technology.

References

1. Gieras, Jacek and Wang, Rong-Jie and Kamper, Maarten, Axial Flux Permanent Magnet Brushless Machines, 01 2008.
2. B. Dehez, F. Baudart, M. Markovic, and Y. Perriard, "Theoretical and experimental investigation of flex-pcb air-gap windings in slotless bldc machines," IEEE Transactions on Industry Applications, vol. 50, no. 5, pp. 3153–3160, 2014.
3. N. Kurita, R. Inomata, W. Gruber, and T. Okayasu, "Examination of flex pcb configuration for a winding of a magnetic levitation motor," in 2020 23rd International Conference on Electrical Machines and Systems (ICEMS), 2020, pp. 1655–1658.
4. Yan G-J, Hsu Wang Tsai Wu L-YJ-HM-CX-Y (2009) Axial-Flux Permanent Magnet Brushless Motor for Slim Vortex Pumps. Magn Ieee Trans 45(11):4732–4735
5. Kahourzade, Solmaz and Mahmoudi, Amin and Ping, Hew Wooi and Uddin, Mohammad Nasir, "A Comprehensive Review of Axial-Flux Permanent-Magnet Machines," Canadian Journal of Electrical and Computer Engineering, vol. 37, no. 1, pp. 19–33, 2014.
6. Mahmoudi, Amin and Kahourzade, Solmaz and Abd Rahim, Nasrudin and Hew, Wooi and Uddin, Mohammad, "Design and prototyping of an optimised axial-flux permanent-magnet synchronous machine," Electric Power Applications, IET, vol. 7, pp. 338–349, 05 2013.
7. N. S., S. P. Nikam, S. Singh, S. Pal, A. K. Wankhede, and B. G. Fernandes, "High-speed coreless axial-flux permanent-magnet motor with printed circuit board winding," IEEE Transactions on Industry Applications, vol. 55, no. 2, pp. 1954–1962, 2019.
8. Hufschmid M (2021) Grundlagen der Elektrotechnik: Einführung für Studierende der Ingenieur- und. Naturwissenschaften. Springer Fachmedien Wiesbaden, Wiesbaden. https://doi.org/10.1007/978-3-658-30386-0
9. Freescale Semiconductor . (2013) PMSM Electrical Parameters Measurement. https://www.nxp.com/docs/en/application-note/AN4680.pdf. Accessed 10 June 2021

David Auer, received the B.Sc. degree in electrical engineering from Graz University of Technology, Graz, Austria, in 2021. He is currently pursuing his M.Sc. degree in electrical engineering at Graz University of Technology, Graz, Austria.

Stefan Leitner, received the Dipl.-Ing. and Dr. techn. degrees in electrical engineering from Graz University of Technology, Graz, Austria, in 2016 and 2020, respectively. He spent an academic year at the University of Tennessee, Knoxville, USA, in 2014–15, via the International Student Exchange Program (ISEP). He was a visiting scholar at Washington State University, Pullman, WA, USA, and a recipient of the Marshall Plan Scholarship in 2016. He was awarded Oesterreichs Energie-Preis 2017 for his Master's Thesis. His research interests include the design of fractional hp drives, finite element analysis, and microgrids. Mr. Leitner is a member of the Christian Doppler Laboratory for Brushless Drives for Pump and Fan Applications.

Annette Muetze, received the Dipl.-Ing. and the Dr.-Ing. degrees in electrical engineering from Darmstadt University of Technology, Darmstadt, Germany, in 1999 and 2004, respectively, and the Diploma in general engineering from the École Centrale de Lyon, Écully, France, in 1999. She is a Full Professor with the Graz University of Technology, Graz, Austria, where she heads the Electric Drives and Machines Institute. Prior to joining the Graz University of Technology, she was an Assistant Professor at the University of Wisconsin–Madison, Madison, WI, USA, and an Associate Professor at the University of Warwick, Coventry, U.K.